Theor Chem Acc (2012) 131:1236
DOI 10.1007/s00214-012-1236-5

REGULAR ARTICLE

Laser control in open quantum systems: preliminary analysis toward the Cope rearrangement control in methyl-cyclopentadienylcarboxylate dimer

G. Dive · R. Robiette · A. Chenel · M. Ndong · C. Meier · M. Desouter-Lecomte

Received: 29 February 2012 / Accepted: 10 May 2012 / Published online: 8 June 2012

Abstract We present a preliminary simulation toward the control of the Cope rearrangement of the most stable isomer of methyl-cyclopentadienylcarboxylate dimer. An experimental investigation of the dimerization of methyl-cyclopentadienylcarboxylate has been carried out. It shows that the most stable isomer of the dimer, the Thiele's ester, is the major product of the dimerization. The simulation takes it as the initial state for the further control of the Cope reaction. The aim of the simulation is to examine the possibility of laser control to form the target product, not detected during the dimerization. The relevant stationary states have been characterized at the DFT B3LYP level, particularly the Cope transition state in which the dimer is connected only by a single bond r_1. A minimum energy potential surface has been computed in a two-dimensional subspace of two bounds r_2 and r_3 which achieve the dimerization and have a very high weight in the reaction path from the Cope TS to the two adducts. Quantum wave packet optimal control simulation has been studied in a one-dimensional model using an active coordinate $r_- = r_3 - r_2$ which nearly corresponds to the reaction path. The stability of the optimal field against dissipation is examined by a non-Markovian master equation approach, which is perturbative in the system-bath coupling but without limitation on the strength of the field.

Keywords Cope rearrangement · Diels–Alder reaction · Optimal control · Dissipative dynamics · Non-Markovian quantum master equation

Published as part of the special collection of articles celebrating theoretical and computational chemistry in Belgium.

Electronic supplementary material The online version of this article (doi:10.1007/s00214-012-1236-5) contains supplementary material, which is available to authorized users.

G. Dive
Centre d'Ingéniérie des Protéines, Université de Liège,
Sart Tilman, B6, 4000 Liège, Belgium
e-mail: gdive@ulg.ac.be

R. Robiette
Institute of Condensed Matter and Nanosciences,
Université catholique de Louvain,
1348 Louvain-la-Neuve, Belgium
e-mail: raphael.robiette@uclouvain.be

A. Chenel · M. Ndong · M. Desouter-Lecomte (✉)
Laboratoire de Chimie Physique, UMR 8000,
Université de Paris-Sud, 91405 Orsay, France
e-mail: michele.desouter-lecomte@u-psud.fr

A. Chenel
e-mail: aurelie.chenel@ens-cachan.fr

M. Ndong
e-mail: mamadou.ndong@u-psud.fr

C. Meier
Laboratoire Collisions, Agrégats, Réactivité,
UMR 5589, IRSAMC, Université Paul Sabatier,
31062 Toulouse, France
e-mail: chris@irsamc.ups-tlse.fr

M. Desouter-Lecomte
Département de Chimie, Université de Liège,
Sart Tilman, B6, 4000 Liège, Belgium

1 Introduction

Experimental control in condensed phase by feedback loops is now a very efficient technique to modify reactivity

[1]. As discussed in this recent review [1], numerical simulations in complex systems are usually too simplified to be really predictive in laser design since experiments automatically work with exact systems without any knowledge of the molecular Hamiltonian. However, simulations remain important in this context to explore the feasibility of control in different systems, analyze the mechanism and particularly the role of the surrounding. Therefore, to induce future progress in experiment–theory interplay, it is crucial to develop efficient numerical methods to simulate laser control in complex systems.

In this work, we present a preliminary analysis of a possible interesting candidate for a control of a Cope rearrangement in the framework of the Diels–Alder reaction. We focus here on the Cope rearrangement of the dimer of methyl-cyclopentadienylcarboxylate. The first step is an experimental exploring of the dimerization to identify the major adduct and justify that we can take it as the initial state for a further control of its Cope rearrangement. In a second step, a full determination of all minima and transition states (TS) connecting different isomers has been carried out to characterize the reactant and the target for the isomerization control. Finally, we take this molecular system to calibrate a strategy for simulating control in a surrounding. We present here the first results suggesting the feasibility of the control.

Control of isomerization reaction by designed laser pulses in a thermal environment has been frequently investigated since the early days of laser chemistry [2–21]. Isomerization involves transfer from a potential well to another one and different control strategies have been suggested either in the UV domain via the electronic excited states in the pump and dump scheme [6–11] or in the infrared range in the ground electronic state by overcoming the barrier via the delocalized highly excited vibrational states [2–5, 12–21]. We focus here on a particular isomerization involving a Cope rearrangement inspired by a pioneering theoretical investigation about a Cope rearrangement in substituted semibullvalenes [2]. It is well-known that the surface surrounding the Cope transition state (TS) of a pericyclic rearrangement is very flat leading to a large barrier and well-localized vibrational ground states in each well with negligible tunnel effect. Few years ago, we have studied the dynamics of the dimerization of cyclopentadiene in the bifurcating region connecting the TS1 of C_2 symmetry and the Cope TS and examined the possibility of preparing shaped wave packets in this region by optimal control theory (OCT) [22]. Here, we want to control the Cope rearrangement, and therefore, we choose a situation with a substituted cyclopentadiene so that the two isomers connected by the Cope TS are sufficiently different to be easily detected after control. The dimerization of methyl-cyclopentadienylcarboxylate (**1**) can involve different isomers but the major product is known to be Thiele's ester **2a** (Scheme 1) [23]. This ester is the reactant for the control and the target is the product of the Cope rearrangement of this later. An extensive investigation of all the possible conformers has been carried out by quantum chemistry at the B3LYP level to determine the relevant minima and the Cope TS. A two-dimensional potential energy surface in a selected subspace and the dipole moment surfaces have been calculated.

Quantum control by optimally shaped laser pulses exploits fine quantum interferences in the system and is therefore extremely sensitive to decoherence due to the uncontrolled surrounding. We adopt here the optimal control theory (OCT) in which the laser field is optimized on a temporal grid [24]. It is obvious that simulation of control in a complex system must involve a simplified quantum model and the full dimensional potential energy surface is often approximated by the system-bath model of a molecular subsystem bilinearly coupled to a harmonic bath describing the environment [25]. At this stage, different dynamical strategies can be followed: an extensive quantum computation with the multilayer multi-configuration time-dependent Hartree (MCTDH) up to some hundreds of atoms [26] or dissipative dynamics in which the surrounding is taken into account by a global spectral density [27]. Here, we implement a non-Markovian dissipative dynamics in the density matrix formalism valid at the second order in the system-bath coupling but with no limitation on the strength of the field [28]. Such a time non-local non-Markovian approach with a memory including the whole dynamics from the initial time allows that the surrounding and the system have similar dynamical timescales leading to easy energy exchanges. Following the particular Meier–Tannor parameterization of the spectral density of the bath [28–30], the field-dressed dissipation is treated by a set of auxiliary matrices implicitly containing the memory terms and coupled to the system. This leads to a local dynamics which remains, however, difficult to manage numerically and up to now has been applied on model or small systems. Our aim is to calibrate the auxiliary matrix

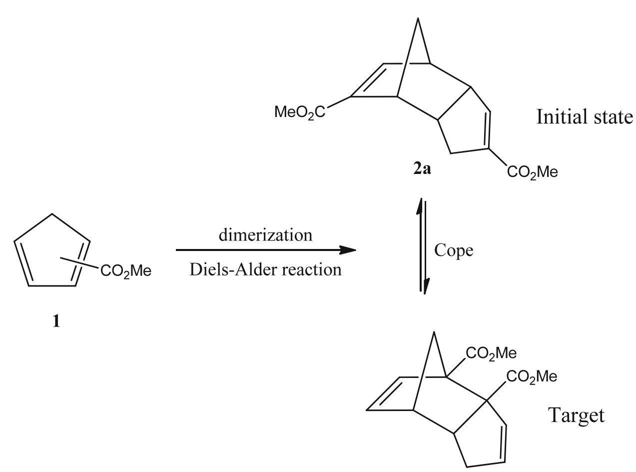

Scheme 1 Formation of dimer **2a** and its Cope rearrangement

Scheme 2 Synthesis and dimerization of methyl-cyclopentadienylcarboxylate

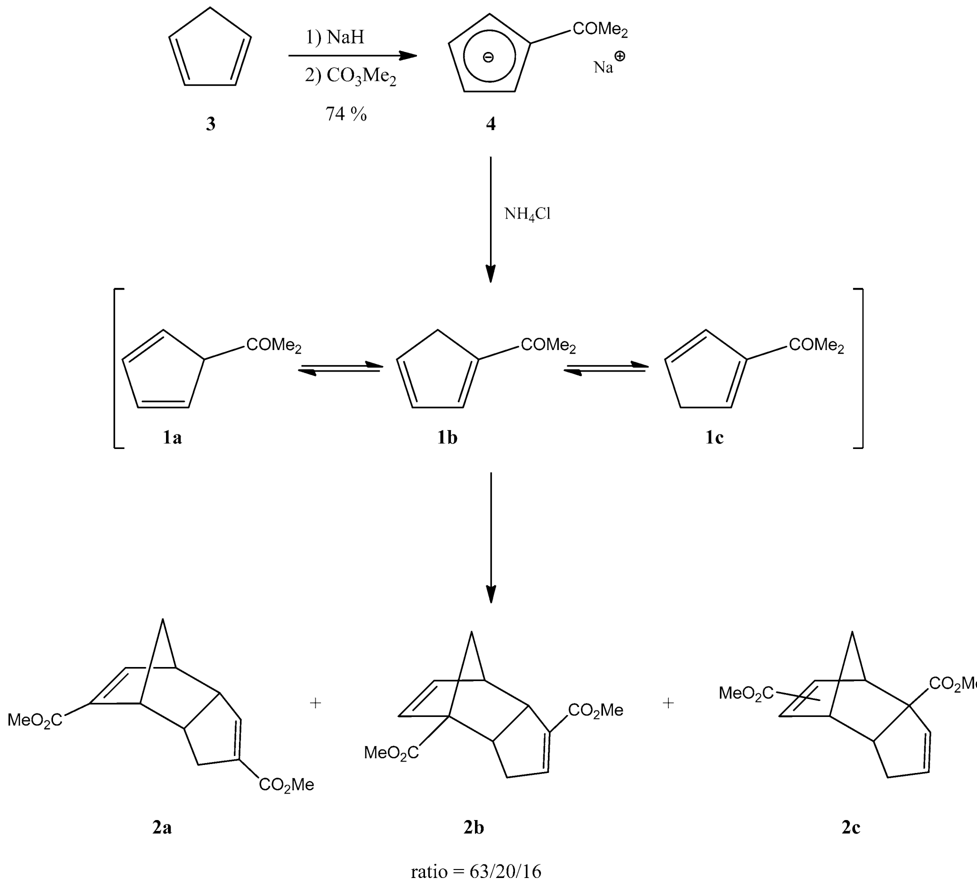

method in a large system. We begin by an analysis of a one-dimensional model along a particular scan connecting the reactant and the target. An optimal field is designed in the system and we analyze the stability of the control in various environments with different frequency cutoffs, coupling strengths and temperatures. In this work, we want to concentrate on the dissipation effects on an optimal control field. To this end, an optimal control field was constructed without the influence of the bath, and subsequently, in a second step used in a dissipative environment. The inclusion of the bath into the control scenario and thus the study to which extent optimal control theory can compensate for dissipative effects is the subject of current studies, which will be presented on the future.

2 Chemistry of dimerization

The aim of this experimental section is (1) to justify that it is realistic to propose Thiele's ester as the initial state of an isomerization laser control because it is the major adduct of the dimerization of methyl-cyclopentadienylcarboxylate, (2) develop reaction conditions and (3) fully characterize all the products of the dimerization. The monomer exists in three tautomeric forms (**1a**, **1b**, and **1c**; Scheme 2) which are in rapid equilibrium [31]. It is well-known that this species is highly reactive and undergoes dimerization (via a Diels–Alder cycloaddition) to yield Thiele's ester (**2a**) [23, 32–34].

Since its high reactivity, methyl-cyclopentadienylcarboxylate (**1**) cannot be isolated and must be synthesized in situ, just prior to its use. We thus have prepared the corresponding anion, lithium carbomethoxycyclopentadienide (**4**), by treatment of cyclopentadiene with sodium hydride in THF, followed by addition of dimethyl carbonate [35]. This procedure gives cyclopentadienide **4**, which is stable and can be stored for months, in 74 % yield. Formation of diene **1** was performed by adding a saturated solution of NH_4Cl to a dichloromethane solution of **4**. Under these conditions, anion **4** undergoes a rapid protonation to yield the desired methyl-cyclopentadienylcarboxylates (**1a–c**). As mentioned previously, these later are highly reactive and undergo a rapid dimerization (by Diels–Alder reaction). Previous reports indicate that after purification this experiment affords Thiele's ester [32–34]. However, analysis of the crude mixture revealed that there is not just one product which is formed but three (**2a**, **2b**, and **2c**) in a 63/20/16 ratio. These three adducts could be separated by column chromatography and analyzed by nuclear magnetic resonance (NMR), high resolution mass spectrometry (HRMS) and infrared spectroscopy (see Electronic Supplementary Material).

First, [1]H and COSY NMR analysis of the major product showed a perfect concordance with reported data [36] and confirmed that it is Thiele's ester (**2a**). HRMS analysis then confirmed the $C_{14}H_{16}O_4$ molecular formula for the two minor compounds; these later being thus indeed also dimeric forms. A detailed NMR study ([1]H, [13]C, COSY, HMQC, HMBC) of these two compounds allowed identifying **2b** and **2c** as possessing the structure showed in Scheme 2 (the localization of the ester function on the double bond in **2c** could not be determined).

It is important to note that these two isomers (**2b** and **2c**) do not come from the same arrangement of reactants as the one leading to Thiele's ester or the product of its Cope rearrangement. And this later could not be detected in the crude mixture.

3 Quantum chemistry investigation

All the calculations have been performed with the Gaussian suite of programs [37] at the B3LYP level [38] using the double ζ basis set 6-31G(d) [39]. As described by Spino et al. [31], methyl-cyclopentadienylcarboxylate can exist in three equilibrium isomers noted **1a**, **1b**, and **1c** but only a combination of the diene with the ester in the 2-position (**1c**) and 1 position (**1b**) could give rise to the Thiele's ester adduct [23]. **2b** and the two forms of **2c** products are 4.2 and 4.5/4.9 kcal less stable than **2a**. It can be noted that the heat of formation is higher for **2a** (16.6 kcal) than the one for **2b** (12.4 kcal) and **2c** (13.9/13.5 kcal).

This Diels–Alder reaction can be described as a two-step mechanism as previously analyzed in the dimerization of unsubstituted cyclopentadiene [22]. Depending on the conformation of both ester fragments, four geometric arrangements can be obtained as stationary points. All the calculations have retained the most stable one. A first transition state structure (TS1) has been located as for the unsubstituted cyclopentadiene addition with the formation of a single bond between both cycles. This first bond is equal to 2.007 Å and will be noted r_1 It is associated with a imaginary frequency of 369.89 cm^{-1}. Following this coordinate, the Cope TS is reached at $r_1 = 1.644$ Å which is 3.402 kcal more stable than the first transition state (TS1). At that point, the normal mode of the 80.05 cm^{-1} imaginary frequency is associated with the formation the r_2 and r_3 bonds respectively. The adduct with r_1 and r_2 bonds is the Thiele's ester which defines the barrier height of 26.8 kcal (1.16 eV). This minimum is 10.4 kcal (0.45 eV) more stable than the other adduct with r_1 and r_3 bonds. The energy and the values of the three important coordinates r_1 r_2 and r_3 are reported in Table 1. The three equilibrium structures of the Cope TS and the two adducts are depicted in Fig. 1. C_1 and C_2 atoms define the z-axis and the x-axis is in the C_1–C_2–C_3, plane.

Table 1 Energy and geometry of the main stationary points

	TS1	TS cope	Adduct $r_1 - r_2$	Adduct $r_1 - r_3$
E	30.2	26.8	0.0	10.4
r_1	2.0	1.6	1.6	1.6
r_2	3.0	2.7	1.6	3.4
r_3	3.0	2.8	3.5	1.6

E relative energy in kcal with respect to Thiele's ester minimum. Coordinates r_1, r_2, r_3 are in Å

The computed higher stability (by 10.4 kcal/mol) of Thiele's ester as compared to adduct $r_1 - r_3$, and the barrier to isomerization for this latter, suggest that experimentally (at room temperature), among these two adducts, only Thiele's ester should be observed. This in good agreement with our expermiental results which showed the formation of Thiele's ester but did not allow detecting adduct $r_1 - r_3$ in the crude mixture (vide supra).

Starting from the Cope TS structure, IRC has been searched along the forward and reverse directions in mass-weighted cartesian coordinates. The reverse branch could lead to the most stable minimum but stops after six steps. Using the standard Z-matrix, the optimization along all the others coordinates leads to the vicinity of the minimum but stops at r_2 distance equals to 1.693 Å while the adduct distance at equilibrium is 1.57 Å and is 6.0 kcal more stable than this last IRC point. As well in cartesian coordinates or using Z-matrix description, the forward branch comes back and does not go in the hoped direction. In the surrounding of the TS, the surface is particularly flat. To overcome this problem, another starting point has been arbitrarily chosen setting the r_3 distance to 2.6 Å. At that non-equilibrium structure, the Hessian matrix has a negative eigenvalue and the associated eigenvector is mainly defined by r_3. Such a way, the IRC starts in the right direction and stops near the second minimum with $r_2 = 3.43$ Å and $r_3 = 1.63$ Å to be compared to the optimized structure values which are 3.45 and 1.63 Å respectively.

In order to obtain a more complete description of the 1D model, a scan of r_2 and r_3 by steps of 0.5 Å has been performed starting from the TS structure in Z-matrix description without any other constraints up to 1.45 Å for both bonds. This 1D scan well connects the three stationnary points. It can be noted the good agreement between the three bond lengths obtained by the 1D scan and the selected IRC points. The r_1 distance lies in the range of 1.57–1.64 Å at the Cope TS. This scan is the one-dimensional model for the preliminary control of the

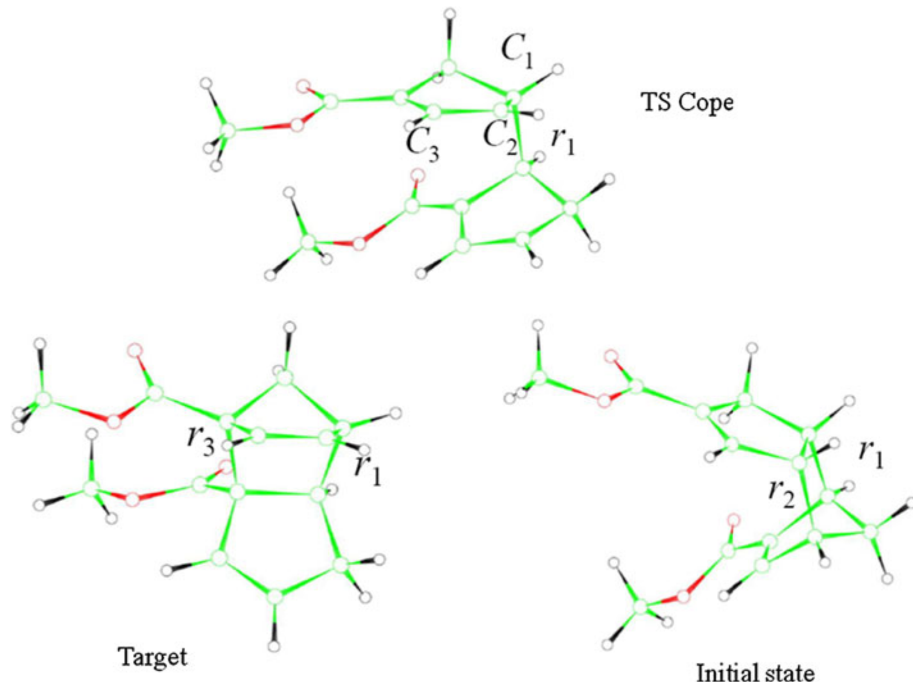

Fig. 1 Equilibrium geometry of the three stationary states involved in the control simulation. *Upper panel*: Cope TS with bond r_1 already formed. *Lower right panel*: Thiele's ester which is the lowest energy adduct obtained by forming the r_2 bond. *Lower left panel*: the target resulting from the formation of the r_3 bond. The atoms noted C_1, C_2 fixes the orientation of the *z*-axis. The *x*-axis is in the plane C_1, C_2, C_3

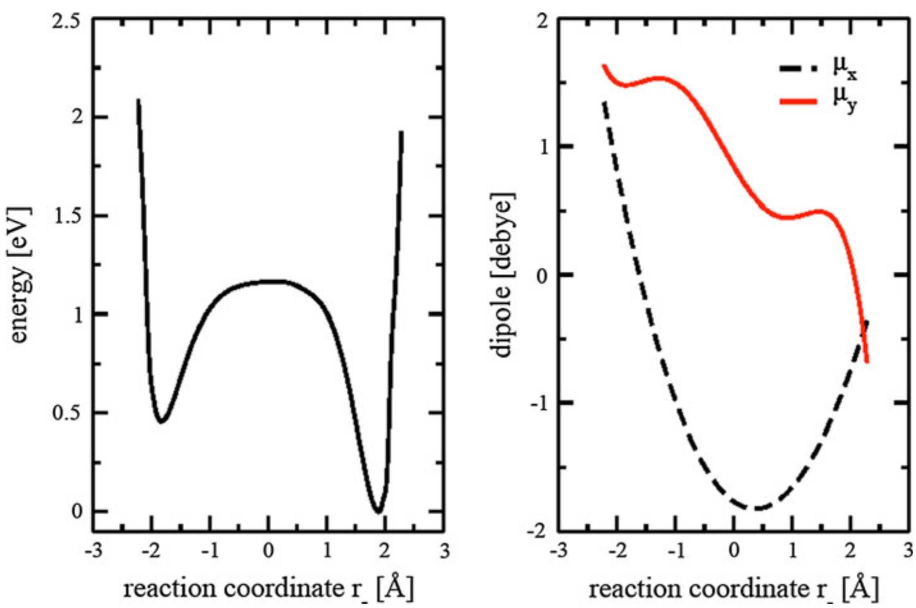

Fig. 2 *Left panel*: one-dimensional minimum potential energy curve along the active coordinate $r_- = r_3 - r_2$, *right panel*: the dipole moment components chosen for the control

rearrangement. The potential energy curve as a function of $r_- = r_3 - r_2$ and two dipole components selected for the control are shown in Fig. 2. Ab initio points are computed in the interval 1.45–3.50 Å and extrapolation is performed in order to get walls for the wave packet dynamics.

Next, a 2D map has been explored in a large range of r_2 and r_3 from 1.2 to 4.6 Å by steps of 0.1 Å by optimization of all the 3 *N*-8 degrees of freedom. This map contains 35 × 35 points. For very short distances, the energy of several points has been extrapolated. For large distances, another problem occurs: r_1 is abruptly broken. Therefore, to obtain a complete map with realistic walls as required for future 2D dynamics which mainly explores the central region of the grid, most of the points of the upper corner have been optimized following r_2 and r_3 with a r_1 distance set just before breaking mainly in the range of 1.7 Å. The map drawn in Fig. 3 have been obtained by the SAS spline fitting procedure [40].

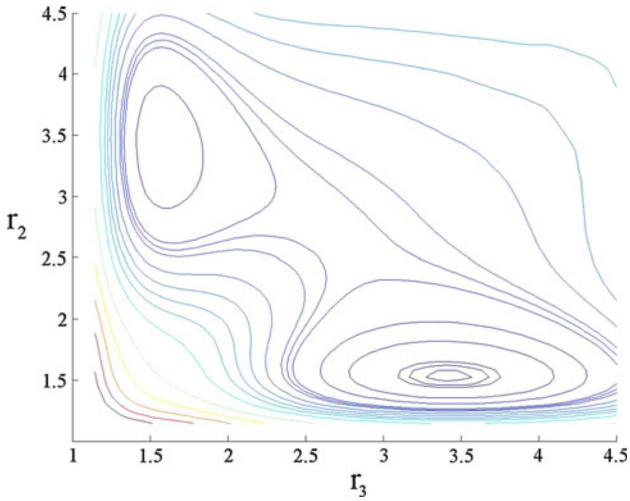

Fig. 3 Minimum energy potential energy surface in the r_2 and r_3 subspace with optimization of all the 3 N-8 degrees of freedom. The energy is given in eV and the successive contours are plot for $E = 0.02$, 0.06, 0.1, 0.4, 0.7, 1.0, 1.1, 1.2, 1.6, 1.9, 2.2, 2.5, 3.0, 3.5, 4.0, 4.5, 6.0, 7.0, and 8.0 eV. Coordinates r_2 and r_3 are in Å

4 Model and methods

4.1 System-bath model

We consider a one-dimensional model with an active coordinate $r_- = r_3 - r_2$. The potential energy $V(r_-)$ curve and the components of the dipole moment are shown in Fig. 2. In the r_2, r_3 subspace, we adopt a Cartesian kinetic energy operator with no cross-term what is justified since both coordinates have no common atom. The corresponding masses are $\mu_2 = \mu_3 = \mu_C/2$ with μ_C being the mass of a C atom. By taking linear combinations $r_- = r_3 - r_2$ and $r_+ = r_3 + r_2$, the kinetic energy remains separable and the part related to the $r_- = r_3 - r_2$ coordinate is $T_{r_-} = -\frac{\hbar^2}{2\mu_-}\frac{\partial^2}{\partial r_-^2}$ with $\mu_- = \mu_2/2 = \mu_C/4$. The model Hamiltonian describing the system and the bath is

$$H(t) = H_S(t) + H_B + H_{\mathrm{SB}} + H_{\mathrm{ren}} \tag{1}$$

with $H_S(t) = T_{r_-} + V(r_-) + W(r_-, E(t))$ where $W(r_-, E(t)) = -\sum_j \mu_j(r_-)E_j(t)$ describes the light-matter interaction at the electric dipolar approximation and j denotes the chosen linear polarizations of the field. In this expression, $H_B = \sum_{i=1}^{N}\left(T_i + m_i\omega_i^2 q_i^2/2\right)$ is a collection of harmonic oscillators which mimic the effects of the remaining modes and the solvent environment. We choose a bilinear coupling $H_{\mathrm{SB}} = -\sum_{i=1}^{N} c_i q_i r_-$ of the system degree of freedom to the modes of the model environment, which leads to a renormalization term $H_{\mathrm{ren}} = Cr_-^2/2$ with $C = \sum_{i=1}^{N} c_i^2/m_i\omega_i^2$. The coupling to the environment is determined by the coupling coefficients c_i, the distribution of which is given by the spectral density defined as

$$J(\omega) = \frac{\pi}{2}\sum_{i=1}^{N}\frac{c_i^2}{m_i\omega_i}\delta(\omega - \omega_i). \tag{2}$$

Within a perturbative approach, which is second order in the system-bath coupling, the entire bath dynamics enters into the system dynamics via the complex bath correlation function, defined by

$$C(t) = \frac{1}{2\pi}\int_{-\infty}^{\infty} \mathrm{d}\omega J(\omega)[\cos(\omega t)\coth(\beta\omega/2) - i\sin(\omega t)] \tag{3}$$

with $\beta = 1/k_B T$.

4.2 Auxiliary density matrix method

Open systems are generally described within the density matrix formalism [27–30, 41, 42]. The reduced density matrix $\rho_S(t)$ associated with the system is obtained by tracing over the bath coordinates. In the Nakajima–Zwanzig formalism [43], $\rho_S(t)$ is solution of a reduced equation containing a memory which depends on the whole history of the global system-bath

$$\dot{\rho}_S(t) = L_{\mathrm{eff}}\rho_S(t) + \int_0^t \mathrm{d}t' K(t,t')\rho_S(t') \tag{4}$$

where we have supposed a factorizing initial condition and where $L_{\mathrm{eff}}\cdot = -i[H_S(t) + H_{\mathrm{ren}}, \cdot]$ with $\hbar = 1$ and $[\cdot,\cdot]$ designates the commutator. Within the weak system-bath coupling (but not the light-matter interaction), the second-order perturbation gives a tractable expression for the memory kernel in which the bath only enters via its correlation function $C(t)$ and its Hermitian conjuguate $\bar{C}(t)$ [28–30, 38, 39]

$$K(t,t')\rho_S(t') = -\left[x, C(t-t')\mathrm{e}^{L_S(t-t')}x\rho_S(t')\right] + \left[x, \bar{C}(t-t')\mathrm{e}^{L_S(t-t')}\rho_S(t')x\right] \tag{5}$$

where we have noted x the active coordinate of the system ($x = r_-$ in our case) and $L_S\cdot = -i[H_S(t), \cdot]$. The basic efficient idea of the auxiliary matrix method is to propose a particular parameterization of the spectral density [28] as a combination of Lorentzian functions so that $C(t)$ can be expressed as a sum over the poles in the complex plane and takes a simple expression

$$C(t-t') = \sum_{k=1}^{n} C_k(t-t') = \sum_{k=1}^{n}\alpha_k \mathrm{e}^{i\gamma_k(t-t')} \tag{6}$$

A detailed derivation of these relations is given in Ref. [30]. By inserting this expression for $C(t)$, the integral of the memory term is split into a sum of contributions for each component k of the correlation function and each partial integral is set equal to an auxiliary matrix

$$\rho_k(t) = i\alpha_k \int_0^t \mathrm{d}t' \mathrm{e}^{i\gamma_k(t-t')} \mathrm{e}^{L_S(t-t')} x \rho_S(t') \tag{7}$$

By taking the time derivative of this integral, one obtains a set of coupled equations for the density matrix of the system $\rho_S(t)$ and the n auxiliary matrices $\rho_k(t)$. The main point is that this technique allows us to carry out non-Markovian dynamics by a system of coupled equations local in time.

At this stage, our contribution is an exploration of different numerical methods to get a stable solution in a molecular system involving many states. Different strategies exist to write the coupled system depending on the definition of the auxiliary matrices and the parameterization of $C(t-t')$ and $\bar{C}(t-t')$. Two different matrices can be connected to the real and imaginary part of each contribution $C_k(t-t')$ [29] or, as discussed in Ref. [30], we can attach only one matrix to each contribution $C_k(t-t')$ but still consider two possibilities for $\bar{C}(t-t')$. We present here only the working equations for which we have obtain stable numerical results. We use

$$\bar{C}(t-t') = \sum_{k=1}^{n} \bar{\alpha}_k e^{i\gamma_k(t-t')} \tag{8}$$

with the same γ_k as in Eq. (6). Then the equations take the form

$$\dot{\rho}_S(t) = L_{eff}\rho_S(t) + i\sum_k [x,\ \rho_k(t)] \tag{9}$$

$$\rho_k(t) = i\int_0^t dt' e^{i\gamma_k(t-t')} e^{L_s(t-t')} (\alpha_k \rho_s(t') - \bar{\alpha}_k \rho_s(t')x)$$

$$\dot{\rho}_k(t) = (i\gamma_k + L_S)\rho_k(t) + i[\alpha_k x \rho_S(t) - \bar{\alpha}_k \rho_S(t) x] \tag{10}$$

Finally, we give the operational relations for the α_k and the γ_k. If the spectral density is fitted by m Lorentzian functions

$$J(\omega) = \frac{\pi}{2}\sum_{k=1}^{m} p_k \frac{\omega}{\left[(\omega+\Omega_k)^2 + \Gamma_k^2\right]\left[(\omega-\Omega_k)^2+\Gamma_k^2\right]} \tag{11}$$

m couples of poles in the evaluation of $C(t-t')$ come from $J(\omega)$. The corresponding coefficients are

$$\begin{aligned} \alpha_{k,1} &= \frac{p_k}{8\Omega_k\Gamma_k}[\coth(\beta(\Omega_k + i\Gamma_k)/2) - 1], \\ \alpha_{k,2} &= \frac{p_k}{8\Omega_k\Gamma_k}[\coth(\beta(\Omega_k - i\Gamma_k)/2) + 1] \\ \gamma_{k,1} &= \Omega_k + i\Gamma_k \text{ and } \gamma_{k,2} = -\Omega_k + i\Gamma_k \end{aligned} \tag{12}$$

Besides, a number of poles in principle infinite but finite in practice for a non-vanishing temperature come from the hyperbolic cotangent function in $C(t-t')$. They are

$$\alpha_k = 2iJ(i\nu_k)/\beta \text{ and } \gamma_k = i\nu_k \tag{13}$$

where $\nu_k = 2\pi(k-m)/\beta$ are the Matsubara frequencies. For $\bar{C}(t-t')$, one must take $\bar{\alpha}_{k,2} = \alpha^*_{k,1}, \bar{\alpha}_{k,1} = \alpha^*_{k,2}$ for $1 < k \leq m$ and $\bar{\alpha}_k = \alpha_k$ for $k > m$ [30].

The coupled equations have been integrated by the split-operator technique [44]. In matrix form, the system reads

$$\begin{pmatrix} \dot{\rho}_S(t) \\ \vdots \\ \dot{\rho}_k(t) \\ \vdots \end{pmatrix} = \begin{pmatrix} L_{eff}(t) & \cdots & L^- & \cdots \\ \vdots & & \vdots & \\ O_k & & L_S(t) + i\gamma_k & \\ \vdots & & \vdots & \end{pmatrix} \begin{pmatrix} \rho_S(t) \\ \vdots \\ \rho_k(t) \\ \vdots \end{pmatrix} \tag{14}$$

where $O_k = \frac{1}{2}[\alpha_k(L^- + L^+) + \bar{\alpha}_k(L^- - L^+)]$ where $O_k = \frac{1}{2}[\alpha_k(L^- + L^+) + \bar{\alpha}_k(L^- - L^+)]$ with $L^- = i[x, .]$ (i.e., a commutator) and $L^+ = i[x, .]_+$ (i.e., an anticommutator). In a more concise form, this can be written as

$$\partial_t \hat{\rho}(t) = \left(L_{\text{diag}} + L_{\text{off}}\right)\hat{\rho}(t)$$

where $\hat{\rho}(t)$ is a vector containing the system $\rho_S(t)$ and auxiliary density matrices $\rho_k(t)$, and L_{diag} and L_{off} are the diagonal and off-diagonal matrix blocks of Eq. (14) containing the operators in Liouville space. By splitting the diagonal and off-diagonal part, one gets $\hat{\rho}(t+\delta t) = e^{L_{\text{off}}\delta t/2} e^{L_{\text{diag}}\delta t} e^{L_{\text{off}}\delta t/2}\hat{\rho}(t)$. The diagonal part is applied on a grid basis set by using the usual fast Fourier transform between the position representation for the potential operator and the impulsion representation for the kinetic operator. The off-diagonal part is treated by a Cayley iteration procedure [29, 45].

4.3 Optimal control

In a preliminary step, the field is designed by optimal control theory without dissipation in the Hilbert space and we examine the stability when dissipative dynamics is used in the Liouville space with different spectral densities and system-bath couplings. Optimizing directly with the auxiliary matrices is in progress for a future work. In the case of the dynamics without dissipation, we can use the standard OCT approach based on the time-dependent Schrödinger equation. The optimal field able to drive the initial wave packet toward the target is determined by variational theory. In reactivity, the functional is usually the probability that the steered wave packet is the target at a given final time $t_{\max}$. The functional is maximized under the constraints that the laser fluence remains acceptable and the Schrödinger equation is satisfied at any time [24]

$$F[E(t)] = \left|\left\langle \psi(t_{\max}) \mid \psi_{\text{target}} \right\rangle\right|^2 - \alpha_0 \int_0^{t_{\max}} dt \sum_j E_j^2(t)$$
$$- 2\Re e\left[\left\langle \psi(t_{\max}) \mid \psi_{\text{target}} \right\rangle \int_0^{t_{\max}} dt \langle \chi(t)|\partial_t\right.$$
$$\left. -i\left(H^0 - \sum_j \mu_j E_j(t)\right)|\psi(t)\rangle\right] \quad (15)$$

with a positive Lagrange multiplier α_0. Varying the functional leads to three coupled equations: the Schrödinger equation for $|\psi(t)\rangle$ with an initial condition $|\psi(t=0)\rangle$ (usual forward propagation), the Schrödinger equation for the Lagrange multiplier $|\chi(t)\rangle$ which must be solved with a final condition $|\chi(t_{\max})\rangle = \left|\psi_{\text{target}}\right\rangle$ so that in practice it is solved by a backward propagation and the optimum field for each polarization j.

$$E_j(t) = -(1/\alpha_0)\Im m\left[\left\langle \psi(t) \mid \psi_{\text{target}}(t)\right\rangle \left\langle \psi_{\text{target}}(t)\middle|\mu_j\middle|\psi(t)\right\rangle\right] \quad (16)$$

The equations are solved by the Rabitz iterative monotonous algorithm [24]. We have used the improvement proposed in Ref. [46]. At each iteration k, the field is given by $E_j^{(k)} = E_j^{(k-1)} + \Delta E_j^{(k)}$ where $\Delta E_j^{(k)}$ is calculated by Eq. (16).

5 Results

In this section, we present the results for the laser control of the isomerization of Tiele's ester by a Cope rearrangement. Specifically, the aim is to design laser pulses which, when interacting with the sample, induce an isomerization from the Thiele's ester form (**2a**) to the product of its Cope rearrangement, noted target in Scheme 1, with the corresponding geometries given in Fig. 1. In what follows, we show that the interaction with specifically shaped laser pulses can indeed induce this isomerization reaction (Cope rearrangement), and thus produce a high yield of this molecule. Within this context, the influence of the surrounding bath plays a key role, and its effects are studied in detail in Sect. 5.2.

5.1 Control without dissipation

Only the ground vibrational state of the reactant is populated at room temperature since the energy gap between the two wells is 0.453 eV. One can consider that the initial ensemble is a pure case. The initial state is then this first vibrational eigenvector $|\psi(t=0)\rangle = |\phi_{n=1}\rangle$ where the n labels the eigenvectors. The ground state of the second well is the fifth eigenvector $\left|\psi_{\text{target}}\right\rangle = |\phi_{n=5}\rangle$. We optimize a field with a duration $t_{\max} = 5\,ps$ as short as possible taking into account a limiting value of the field amplitude of about 0.02 a.u. (1.028×10^8 Vcm^{-1}) to avoid strong fields able to ionize the molecule and to justify the neglect of polarization effects. We take two linear polarizations along directions x and y after an analysis of the dipole matrix elements. As usually in control theory the molecules are assumed to be oriented in the laboratory else we must admit that the field acts on the molecules well oriented in the ensemble. The trial field is chosen so that the localized vibrational states in the initial well up to the middle of the barrier are early populated in order to initiate the heating. Then the OCT finds the field able to cool the wave packet in the second well. The trial field is given by $E_j^{(0)}(t) = \varepsilon_0 s(t) \sum_{k=1}^{n_j} \cos(\omega_k t)$ with $j = x,\ y$. We choose three frequencies for the x polarization, ω_{12} (1,027.0 cm^{-1}), ω_{23} (1,004.6 cm^{-1}), ω_{34} (977.7 cm^{-1}) and two for y, ω_{46} (943.2 cm^{-1}), ω_{68} (892.0 cm^{-1}) with an amplitude $\varepsilon_0 = 10^{-2}$ a.u. (5.142×10^7 Vcm^{-1}). $s(t) = \sin^2(\pi t/t_{\max})$ is a smooth switching function. The fidelity defined by the probability to be in the target state at the end of the pulse $f = \left|\left\langle \psi(t_{\max}) \mid \psi_{\text{target}}\right\rangle\right|^2$ converges at 99.9 % after about 200 iterations. However, to force a limit maximum field amplitude, we divide the amplitude by a factor two and let iterate again for 100 iterations. This process is repeated twice. The final optimal field is drawn in Fig. 4 with its Fourier transform in which we find the zero-order frequencies mainly used for heating and all the other ones obtained by OCT to drive the wave packet in the delocalized states and to cool it toward the target.

Figure 5 gives the evolution of the population in the initial state and in the target as well as in some transitorily populated states during the control. The states belonging to the reactant well are drawn in full lines, those of the target well in dashed lines and the delocalized states in dots. At the beginning, the heating mainly populates the excited states of the reactant well using mainly the transitions proposed by the trial field. Then few highly delocalized states are transitorily populated and the OCT algorithm finds the transitions efficient for the cooling from the delocalized states. Some high frequencies appear in the Fourier transform of the field corresponding to very highly excited states but the probability remains very small and is not drawn in Fig. 5.

5.2 Stability of the control under dissipation

The optimal field is used to propagate the coupled system of auxiliary matrices by varying the spectral density of the

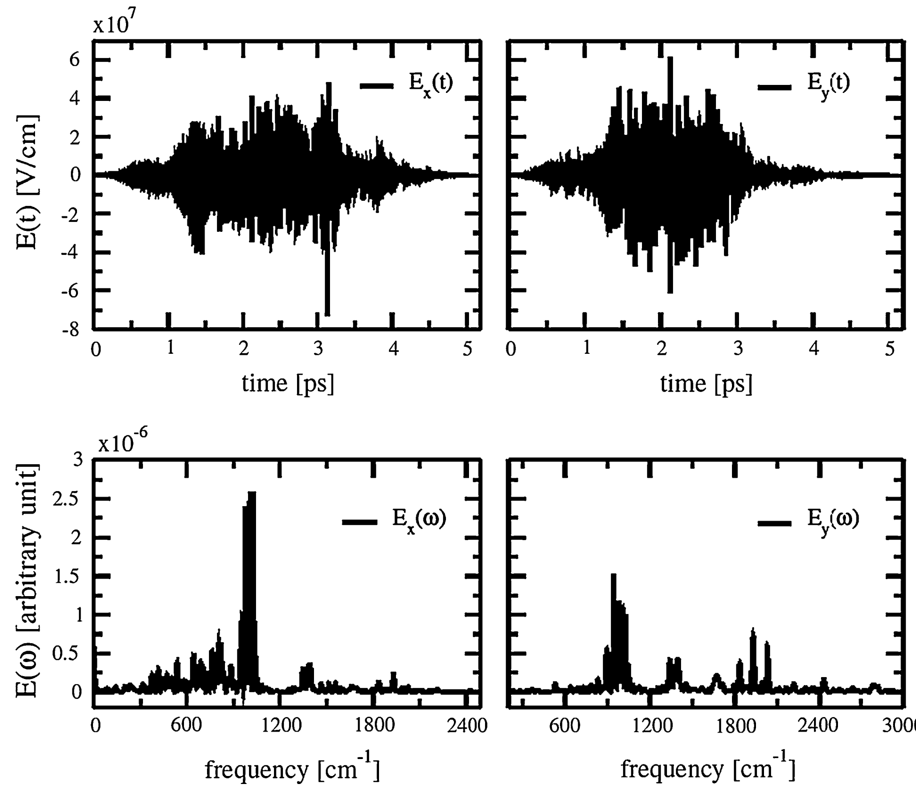

Fig. 4 Optimal field driving the isomerization in the 1D model without dissipation and the corresponding Fourier transforms

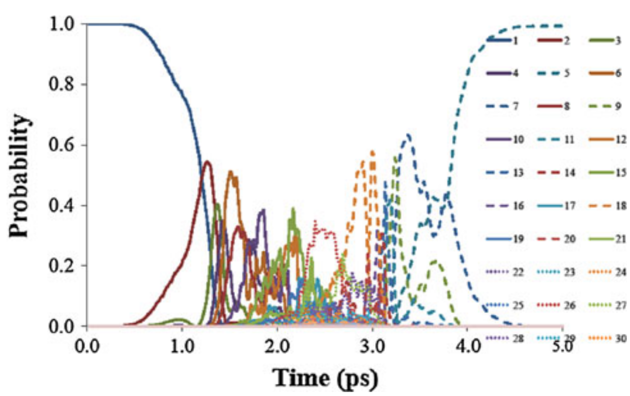

Fig. 5 Probability of populating the eigenstates of the 1D model during the control without dissipation. *Full lines*: states of the reactant well, *dashed lines*: states of the target well, *dots*: delocalized states

Table 2 Fidelity $f = \left|\left\langle \psi(t_{\max}) \mid \psi_{target} \right\rangle\right|^2$ of the control in % for different temperatures, cutoff frequencies ω_c and system-bath couplings λ (Eq. 17)

λ	300 K		200 K		100 K	
	10^{-3}	5×10^{-4}	10^{-3}	5×10^{-4}	10^{-3}	5×10^{-4}
ω_c (cm^{-1})						
400	84.7	91.9	89.1	94.3	93.7	96.7
900	83.3	91.1	87.8	93.6	92.3	96.0
1,700	80.6	89.7	85.9	92.8	88.7	96.3

bath. The spectral density is taken to be Ohmic with a high-frequency cutoff ω_c

$$J(\omega) = \lambda\omega e^{-\omega/\omega_c} \tag{17}$$

This is fitted to the functional form of Eq. (11) with a single set of parameters k. We examine three cutoff frequencies ($\omega_c = 400$, 900 and 1,700 cm^{-1}), two coupling strengths ($\lambda = 10^{-3}$ and 5×10^{-4}) and three temperatures. The coupled system of auxiliary matrices is solved with 5, 10, and 15 Matsubara frequencies for $T = 300$, 200, and 100 K, respectively. The fidelities of the control are summarized in Table 2. As expected, the control field optimized without surrounding cannot achieve a perfect fidelity when dissipation occurs. However, we have selected examples showing that control is not completely destroyed and that in the context of reactivity an acceptable ratio can be obtained.

Upper left panel of Fig. 6 shows the evolution of the average energy of the field free system $\bar{E} = Tr[(T_{r_-} + V(r_-))\rho_S(t)]$ during the process and the upper right panel gives $Tr\left[\rho_S^2(t)\right]$ which is a measure of the decoherence of the quantum system. Lower panels of Fig. 6 show the Gabor transform of the field indicating when the frequencies appear in time

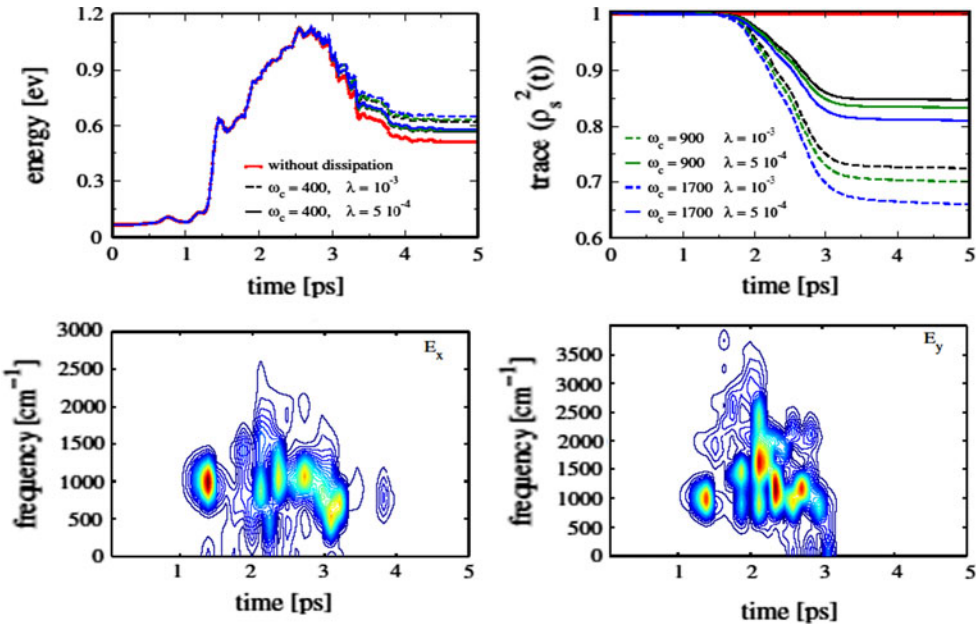

Fig. 6 Dissipative dynamics of the system for different cut-off frequencies ω_c and coupling λ (Eq. 17) at $T = 300$ K. The system is driven by the control field optimized without surrounding. *Left upper panel*: average energy $\bar{E} = Tr[(T_{r_-} + V(r_-))\rho_S(t)]$ of the field free system, *right upper panel*: measure of the purity of the system $Tr\left[\rho_S^2(t)\right]$. *Lower panels*: Gabor transform (Eq. 18) of the field showing when the frequencies operate during the process

$$F(\omega, t) = \left| \int_{-\infty}^{+\infty} H(s - t, \tau) E(s) e^{i\omega s} ds \right|^2 \tag{18}$$

where $H(s,\tau)$ is the Blackman window [47] $H(s, \tau) = 0.08\cos(4\pi s/\tau) + 0.5\cos(2\pi s/\tau) + 0.42$ if if $|s| \leq \tau/2$ and $H(s, \tau) = 0$ elsewhere and τ is the time-resolution chosen to be $\tau = 0.2$ ps. As shown also in Fig. 4, one sees that the process involves frequencies below 3,000 cm^{-1} and mainly frequencies around 1,000 cm^{-1}. They operate principally between 1.5 and 3.5 ps, thus during the crossing of the barrier. As a consequence, for a low value of the cutoff, the main frequencies experience a smaller effect of the surrounding bath, which is clearly confirmed by the results presented on Table 2. As expected, a higher temperature or an increased coupling strength also increases the dissipative effects, with the consequence that fidelity of the control, which was close to 100 % in the dissipative-free case, drops to about 80 % for the values $\omega_c = 1{,}700\ \text{cm}^{-1}$, $T = 300$ K and $\lambda = 10^{-3}$. This increased dissipative effects are also seen as a loss of the purity measured by $Tr\left[\rho_S^2(t)\right]$, given in Fig. 6 (right upper panel). Interestingly, in Fig. 6 (left upper panel), we find that the initial heating process is less affected by the dissipation than the subsequent cooling. Besides, the fact that dissipative effects accumulate in time, one reason could be that the isomerization proceeds via strongly delocalized states (see Fig. 5), which experience a higher degree of dissipation due to the position dependent coupling to the bath. To which extent an approach which includes dissipation at the design stage can compensate for this effect is currently under investigation.

6 Conclusion

We have presented preliminary studies toward the laser control of a Cope rearrangement in a realistic molecular system.

Our experimental study of the dimerization of methylcyclopentadienylcarboxylate (**1**) allowed identifying and characterizing all the products of the reaction. The process predominantly leads to Thiele's ester (**2a**), but the product of its Cope rearrangement could not be detected in the crude mixture.

The control process under study is the further isomerization of Thiele's ester at room temperature. In order to theoretically assess the possibility of laser control of this reaction, we have in a first step analyzed the reaction path and the transition state using high-level quantum chemistry methods. Based on these results, we have constructed a one- and two-dimensional model where the bond lengths r_2 and r_3 which achieve the dimerization after the Cope TS, are chosen as dynamical variables, the most representative ones of the motion along the reaction path. The one-dimensional model was used to theoretically construct a control field using optimal control theory. To assess the effect of a dissipative environment, we have applied the obtained optimal control field within a dissipative quantum propagation using a non-Markovian master equation approach. As expected, the control yield drops for an increasing dissipation. However, the objective chosen in our example retained a high degree of controllability, an encouraging result in view of a possible experimental realization. The next steps in our study consist in extending the control calculation to the proposed two-dimensional model. Furthermore, a very interesting aspect is the inclusion of the dissipation at the design step of the control field, to explore to which extent the external laser field can compensate, at least partially, for the dissipative effects caused by the environment. Studies along this line are currently in progress.

Acknowledgments Dr. G. Dive and Pr. R. Robiette are research fellows of the F.R.S.-FNRS of Belgium. The financial support of the F.R.S for the access to the HPC facilities installed at ULg and UCL is greatly acknowledged. This work was supported by the COST Action CM0708 CUSPFEL.

References

1. Brif C, Chakrabarti R, Rabitz H (2010) New J Phys 12:075008–075068
2. Korolkov MV, Manz J, Paramonov GK (1996) J Chem Phys 105:10874–10889
3. Došlić N, Sundermann K, González L, Mó O, Giraud-Girard J, Kühn O (1999) Phys Chem Chem Phys 1:1247–1257
4. Kühn O (2002) J Phys Chem A 106:7671–7679
5. Hoki K, Ohtsuki Y, Fujimura Y (2001) J Chem Phys 114:1575–1581
6. Vogt G, Krampert G, Niklaus P, Nuemberger P, Gerber G (2005) Phys Rev Lett 94:068305-4
7. Hoki K, Brumer P (2005) Phys Rev Lett 95:168305-4
8. Vogt G, Nuernberger P, Brixner T, Gerger G (2006) Chem Phys Lett 433:211–215
9. Kotur M, Weinacht T, Pearson BJ, Matsika S (2009) J Chem Phys 130:134311-5
10. Mitrić R, Petersen J, Bonačić-Koutecký V (2009) Phys Rev A 79:053416-6
11. Prokhorenko VI, Halpin A, Johnson PJM, Dwayne Miller RJ, Brown LS (2011) J Chem Phys 134:085105-10
12. Sha SP, Rice SA (2000) J Chem Phys 113:6536–6541
13. Gong J, Ma A, Rice SA (2005) J Chem Phys 122:204505-5
14. Zhang M, Gong J, Ma A, Rice SA (2007) J Chem Phys 127:144501-9
15. Artamonov M, Ho T-S, Rabitz H (2006) J Chem Phys 124:064306-10
16. Artamonov M, Ho T-S, Rabitz H (2006) Chem Phys 328:147–155
17. Sugny D, Kontz C, Ndong M, Justum Y, Dive G, Desouter-Lecomte M (2006) Phys Rev A 74:043419-14
18. Gräfe S, Meier C, Engel V (2007) J Chem Phys 122:184103-8
19. Cheng T, Darmawan H, Brown A (2007) Phys Rev A 75:013411-11
20. Kondorskiy A, Nakamura H (2008) Phys Rev A 77:043407-8
21. Kurosaki Y, Artamonov M, Ho T-S, Rabitz H (2009) J Chem Phys 131:044306-8
22. Lasorne B, Dive G, Desouter-Lecomte M (2005) J Chem Phys 122:184304-10
23. Marchand A, Zhao D, Ngooi T, Vidyasagar V (1993) Tetrahedron 49:2613–2620
24. Zhu W, Botina J, Rabitz H (1998) J Chem Phys 108:1953–1963
25. Garg A, Ohnuchic JN, Ambegaokar V (1985) J Chem Phys 83:4491–4503
26. Westermann T, Brodbeck R, Rozhenko AB, Shoeller W, Manthe U (2011) J Chem Phys 135:184102-12
27. Yan Y, Xu R (2005) Annu Rev Phys Chem 56:187–219
28. Meier C, Tannor DJ (1999) J Chem Phys 111:3365–3376
29. Keinekathöfer U (2004) J Chem Phys 121:2505–2514
30. Pomyalov A, Meier C, Tannor DJ (2010) Chem Phys 370:98–108
31. Spino C, Pesant M, Dory Y (1998) Angew Chem Int Ed 37:3262–3265
32. Thiele J (1901) Ber 34:68
33. Peters D (1959) J Chem Soc 1761–1765
34. Dunn GL, Donohue JK (1968) Tet Lett 31:3485–3487
35. Rippert AJ, Hansen H-J (1995) Helv Chem Acta 78:238–241
36. Minter DE, Marchand AP, Lu S (1990) Magn Reson Chem 28:623–627
37. Gaussian 09, Revision A.1, Frisch MJ, Trucks GW, Schlegel HB, Scuseria GE, Robb MA, Cheeseman JR, Scalmani G, Barone V, Mennucci B, Petersson GA, Nakatsuji H, Caricato M, Li X, Hratchian HP, Izmaylov AF, Bloino J, Zheng G, Sonnenberg JL, Hada M, Ehara M, Toyota K, Fukuda R, Hasegawa J, Ishida M, Nakajima T, Honda Y, Kitao O, Nakai H, Vreven T, Montgomery Jr JA, Peralta JE, Ogliaro F, Bearpark M, Heyd JJ, Brothers E, Kudin KN, Staroverov VN, Kobayashi R, Normand J, Raghavachari K, Rendell A, Burant JC, Iyengar SS, Tomasi J, Cossi M, Rega N, Millam JM, Klene M, Knox JE, Cross JB, Bakken V, Adamo C, Jaramillo J, Gomperts R, Stratmann RE, Yazyev O, Austin AJ, Cammi R, Pomelli C, Ochterski JW, Martin RL, Morokuma K, Zakrzewski VG, Voth GA, Salvador P, Dannenberg JJ, Dapprich S, Daniels AD, Farkas Ö, Foresman JB, Ortiz JV, Cioslowski J, Fox DJ, Gaussian, Inc., Wallingford CT (2009)
38. Becke AD (1993) J Chem Phys 98:5648–5652
39. Francl MM, Pietro WJ, Hehre W, Binkley J, DeFrees D, Pople JA, Gordon M (1982) J Chem Phys 77:3654–3665
40. SAS 9.1 licenced to University of Liège; copyright (c) 2002–2003 by SAS Institute Inc., Cary, NC, USA
41. Ohtsuki Y (2001) J Chem Phys 119:661–671
42. Xu R, Yan Y, Ohtsuki Y, Fujimura Y, Rabitz H (2004) J Chem Phys 120:6600–6608
43. Breuer H-P, Petruccione F (2003) The theory of open quantum systems. Wiley, New-York
44. Feit MD, Fleck JA, Steiger A (1982) J Comput Phys 47:412–433
45. Press WH, Flannery BP, Teukolsky SA, Vetterling WT (1989) Numerical Recipes. Cambridge University Press, Cambridge
46. Palao JP, Kosloff R (2002) Phys Rev Lett 89:188301-4
47. Sugawara M, Fujimura Y (1994) J Chem Phys 100:5646–5655